

# Magnetic Fields from SOHO/MDI Converted to the Mt. Wilson 150-Foot Solar Tower Scale

Tham Tran, Luca Bertello, Roger K. Ulrich and Scott Evans<sup>1</sup>

*Division of Astronomy, Department of Physics and Astronomy, University of California, Los Angeles, CA 94095-1562*

## ABSTRACT

In order to permit the construction of long-duration time series dependent on the Sun's magnetic field, this paper presents a detailed cross-correlation between sets of simultaneous magnetograms from the Mt. Wilson Observatory (MWO) and the Michelson Doppler Imager (MDI) aboard the SOHO spacecraft. The MWO 150-foot solar tower telescope magnetogram data are for the FeI  $\lambda 525.0$  nm and NiI  $\lambda 676.8$  nm lines and the MDI data are level 1.8 magnetograms also for the NiI  $\lambda 676.8$  nm spectral line. In these comparisons, we apply a saturation correction factor to the MWO  $\lambda 525.0$  nm fields prior to the derivation of the MDI scale factor. Data from March 1997 to August 2002 are used for this work. We have found that the ratio of MWO FeI  $\lambda 525.0$  nm magnetograms over MDI magnetograms is about 1.7, and it is a function of the center-to-limb angle. Moreover, there are differences between the west-side and the east-side ratios, and these differences may come from the angle dependence of the Michelson filters in the MDI instrument. The MDI tuning changes, on the other hand, are not associated with significant jumps in the derived scale factor ratio. The average scale factors should be adequate for the construction of MDI images closely comparable to those of the saturation-corrected long-duration MWO  $\lambda 525.0$  nm sequence.

*Subject headings:* Sun: magnetic fields, Sun: activity, solar wind, solar-terrestrial relations

## 1. Introduction

Solar variability is primarily a consequence of changes in the Sun's large and small-scale magnetic fields. Understanding the influence these variations have on the Earth's climate and near-Earth space environment is a major objective of solar physics. To this end, long-running records of

---

<sup>1</sup>Now at Jet Propulsion Laboratory, Cal Tech, Pasadena, CA

solar magnetic observations have special value and in particular, we wish to maximize the utility of the data from the Mt. Wilson synoptic program of magnetograms from the 150-foot solar tower telescope. Data from this program has been recorded and maintained since 1967. Although periodic improvements have been installed in the system (for a description of the most recent changes see Ulrich et al. 2002), the basic optical system has been retained in as near a stable configuration as possible. While the system is stable and provides a data sequence of good temporal continuity back to 1967, there are several ways in which more recent data sequences of shorter duration provide data that has advantages relative to that from Mt. Wilson. The sequence of magnetograms from the Michelson Doppler Imager instrument (hereinafter referred to as MDI, see: Scherrer et al. 1995) on board the SOHO spacecraft has much better temporal continuity due to the absence of night-time gaps as well as better spatial resolution for each of the images. This paper establishes a relationship between the MDI sequence and the MWO sequence so that the two sets can be merged or compared.

The Sun influences the near-Earth environment through the regularly changing solar wind and through distinct and somewhat unpredictable events such as flares and coronal mass ejections. The need for understanding connections between the Sun and Earth has been laid out by Solar and Space Physics Survey Committee (2003). Progress has been made in using the slowly evolving large-scale magnetic configurations to predict the solar wind speed and the interplanetary magnetic fields (Arge & Pizzo 2000; Hakamada et al. 2002; Arge et al. 2003). Studies using data from solar surface magnetic observations to deduce the larger-scale heliospheric state began with the works of Altschuler & Newkirk (1969) and Schatten et al. (1969) and were followed by a series of papers (Wang & Sheeley 1990b,a; Wang et al. 1991; Wang & Sheeley 1992; Wang et al. 2002) showing that an empirical relationship exists between the solar magnetic fields and the observed solar wind properties. Ultimately the quality of these models is dependent on the observed input data from the solar magnetograms. Because the Zeeman splitting of solar spectral lines depends on: the magnetic structure in the solar atmosphere, the radiative transfer response of the line profile to the split Zeeman components and the response of the observing system to the emergent spectral intensity, the relationship between the reported system magnetic field and the magnetic field in the upper solar atmosphere is different for each instrument system.

Various measures of solar activity – sunspot number, sunspot darkening, plage area, radio frequency flux (10.7 cm), cosmogenic nuclear abundances – have been used to reconstruct the history of Total Solar Irradiance (TSI) going back several hundred years (Solanki & Fligge 2000; Lean 2000b,a). The synoptic magnetic field measurements from MWO are a quantitative record extending back to 1967 and can be used as an anchor to the more recent portions of the reconstructed record. The period during the 20th century is of particular interest since it coincides with the onset of substantial industrial output of greenhouse gases. The reconstructions show that the TSI may also have increased during that era making the disentanglement of the various influencing factors more complicated. Lockwood et al. (1999) suggest that the strength of the coronal magnetic field doubled over 20th century but Arge et al. (2002) used photospheric magnetic field measurements

from MWO, the Wilcox Solar Observatory at Stanford University and the National Solar Observatory to show that at least between 1975 and 2000 the average solar field did not increase and may have decreased. In order to enhance the reliability of studies like this, it is important to increase the number of data bases that can be used. This paper makes it possible to use the data from the MDI system on the same basis as that from the MWO synoptic program.

The Mount Wilson 150-foot solar tower synoptic program of solar magnetic measurements uses the FeI  $\lambda 525.0$  nm spectral line. In 1995, the old MWO optical 4-channel system was replaced by the new 24-channel data-taking system in which the FeI  $\lambda 525.0$  nm observation was to remain consistent with the historic database. The newly introduced 10-point NiI  $\lambda 676.8$  nm line profile allows the direct comparison between the MWO magnetograms and the MDI magnetograms. From that, we can deduce the relationship between the MWO FeI  $\lambda 525.0$  nm magnetograms and the MDI magnetograms.

For this work, we have adopted the approach suggested by Evans (1999) with some modifications in order to generate the simulated MDI magnetogram from the MWO NiI  $\lambda 676.8$  nm observation and the simulated MWO magnetogram from the MDI data. The next two sections of this paper are devoted to a short description of the data and image processing used in our analysis. In section 4 we describe the technique to compute the scale factor between the MDI and MWO magnetograms. Finally, the results are discussed in section 5.

## 2. Data

The detailed description of the MWO synoptic program of solar magnetic observations has been provided in several previous papers (i.e. Ulrich et al. 2002, and references therein). Basically, the 24-channel system at MWO simultaneously observes intensities in 4 spectral lines: the CrII  $\lambda 523.7$  nm, the FeI  $\lambda 525.0$  nm, the Na D  $\lambda 589.6$  nm, and the NiI  $\lambda 676.8$  nm. The spectral sampling is provided by four sets of image reformatters whose entrance apertures are carried on two separately moveable stages. The reformattor for  $\lambda 676.8$  nm samples ten parts of the line while the reformattor for  $\lambda 525.0$  nm samples two. We refer to each reformattor entrance aperture which obtains a slice of the spectrum as a pickup. Magnetograms are obtained either with the 12-arcsecond-square aperture (slowgram) or with the 20-arcsecond-square aperture (fastgram). The polarization modulator alternately selects either a Right Circular Polarization (RCP) or a Left Circular Polarization (LCP) state for the light entering the spectrograph. Magnetic fields are deduced from the inferred Zeeman shift of the spectral line between these two states. The MWO standard magnetogram program and the MDI magnetograms use different methods of carrying out this inference. Owing to the 10-point sampling of the  $\lambda 676.8$  nm line, we can use both the standard MWO method based on two samples at  $\lambda 676.8$  nm  $\pm 2.8$  pm and the MDI method of inference simultaneously. Since the MWO synoptic program baseline magnetograms for  $\lambda 525.0$  nm is also obtained simultaneously, we are able to directly compare the effects of different lines and the effects of different methods of inference.

It takes about 25 minutes to complete one fastgram (the raster scans over the solar disk), and about 45 minutes for one slowgram. Typically, 2 slowgrams and up to 18 fastgrams can be obtained each clear day. For each spectral line, a data file consists of a header, a calibration part, and a main body. The header contains the observed starting and ending times, the spectrograph dispersion in microns per angstrom, the solar radius in encoder units, the observed wavelength, the number of pickups (2 for CrII  $\lambda$ 523.7 nm, 2 for FeI  $\lambda$ 525.0 nm, 10 for Na D  $\lambda$ 589.6 nm, and 10 for NiI  $\lambda$ 676.8 nm), and the positions of the pickups (in microns). The calibration part provides a detailed linescan at each pickup, and these linescans are used to intercalibrate the photomultiplier tube response functions. One set of the NiI  $\lambda$ 676.8 nm linescans on 20 Aug, 2000 at 19:24 UT is shown in figure 1. In this figure, the linescan calibration scaling has been applied and their shapes are nearly indistinguishable. The main body of the magnetogram consists of an irregular grid of data records for which the spatial coordinates in encoder units, the observed time, the Doppler position in microns, and the light intensity measurements for both LCP and RCP of each pixel are provided. The measured points do not fall in a rectangular grid so that some interpolation is required prior to comparison to any solar image for which a square grid is used. In this work, we compare the MWO NiI  $\lambda$ 676.8 nm and the MWO FeI  $\lambda$ 525.0 nm observations to the SOHO/MDI NiI  $\lambda$ 676.8 nm magnetograms.

The MDI magnetograms used in this work are from the dynamics program, which provides the level 1.8 full disk magnetograms, 1024 by 1024 pixel frames with one-minute cadence. A detailed description of the SOHO/MDI instrument can be found in Scherrer et al. (1995). Because MWO magnetograms and MDI magnetograms differ both in spatial resolution and in their time of observation, we have created spectroscopic proxy MDI magnetograms from the MWO NiI on the MWO spatio-temporal grid of  $\lambda$ 676.8 nm observations and proxy MWO pixels from the MDI magnetograms. The spectroscopic proxy of MDI is derived from MWO 10-point spectral information which allows the recreation of the solar spectral line. This simulated solar spectral line is then convolved with the MDI filter functions to recover a model of the MDI measurement. The proxy MWO pixels are derived from the MDI data by temporally interpolating between successive MDI images to reproduce the exact time of each MWO pixel measurement and rebinning the MDI pixels to reproduce the exact position and boundaries of the MWO pixel. Note that the MDI magnetic fields are calculated from the difference between two velocity images each of which depends on four separate filtergrams in a non-linear manner. Consequently, the rebinned magnetic fields may not be the same as magnetic fields derived from rebinned filtergrams. At this stage both proxies are on the MWO spatio-temporal basis. Although the selection of the MWO areas from the MDI images is supposed to reproduce the areas observed by MWO, small scale factor and registration errors persist. In order to remove these, both images are oversampled to a  $512 \times 512$  grid then registered. Finally they are compared pixel-by-pixel to get the cross-correlation and the scale factors as explained in the next two sections. As an important additional step, the MWO FeI  $\lambda$ 525.0 nm magnetograms can be compared directly to the proxy MDI since these are both on the MWO spatio-temporal frame. What we seek is a relationship between the MDI magnetic fields and the MWO  $\lambda$ 525.0 nm magnetic fields. To reach this goal we find the relationship between MDI proxy

of MWO and the MWO proxy of MDI at  $\lambda 676.8$  nm then find the relationship between the MWO proxy of MDI and the MWO magnetic field at  $\lambda 525.0$  nm. Thus the MWO proxy of MDI serves as an intermediary which is not needed by itself. The advantage of using the proxy MDI is to avoid the interpolation of Mt. Wilson 5250 dataset which produces a systematic error in the analysis when compared to the approach followed in the paper. The cause, we believe, is because the MWO 5250 magnetograms had been corrected for the center-to-limb as well as the saturation effect, while the MWO 6768 and the MDI are not. These corrections are not linear and produce a bias in the calculated scale factors as discussed in section 5.

We have selected about 500 MWO NiI  $\lambda 676.8$  nm magnetograms (and the corresponding MWO FeI  $\lambda 525.0$  nm data sets as well as the MDI magnetograms) from March 1997 to August 2002 for this analysis. In order to minimize the mirror polarization effect on the MWO magnetograms caused by the MWO optical system, all selected magnetograms are in the UT range between 18:00 and 22:00.

### 3. Image Processing

#### 3.1. Create Proxy MDI from MWO NiI $\lambda 676.8$ nm Data

The MWO system admits light from a rectangular area on the solar image into the 75-foot spectrograph. The dispersed light is sampled by a set of fiber-optic bundles which are carried on a stage which is servoed to keep the absorption line centered on the fiber-optic bundles. The stage position is recorded along with the observed intensity for each spectral sample at each MWO pixel on the solar surface. Using knowledge of this position along with knowledge of the Sun-MWO velocity as a function of time we can recover the intensity as a function of wavelength in the reference frame of the SOHO spacecraft. Due to the absence of an absolute wavelength reference for both MWO and MDI there is an unknown additive offset velocity that needs to be eliminated in the comparison. The MDI system includes a tunable waveplate system to compensate for the orbital motion and instrument drifts. These are adjusted in such a way as to maintain the four primary filter positions at a wavelength which is as close as possible to being centered on the solar absorption line (Evans 1999, see figure 3.3).

The Babcock magnetogram of the MWO system utilizes two moveable stages, each of which has two sets of fiber-optic bundles sampling the spectral regions near two lines of interest. The output from each fiber-optic bundle in the set is directed onto a photomultiplier tube whose electrical output is digitized by a voltage to frequency converter. A calibration scan is carried out at the beginning of each magnetogram in order to establish the geometric relationship between the input pickups and to normalize the outputs to a common scale where the continua coincide. For this calibration scan the stage is driven quickly past the solar line so that each pickup can measure the same intensity in turn. The calibration scan output is a set of ten arrays of intensity versus stage position in microns. The zero point of this scale is arbitrarily set as the stage position when the

system is initialized. Figure 1 shows the ten calibration scans along with the determined location for each of the pickups. During the scanning of the Sun, the position of the stage carrying the pickups is servo controlled to follow the line motion. The profile we seek is that which would be obtained by a stationary spectral sampling system so that each spectral observation is numerically shifted to a fixed position by interpolation. For this project we concentrate on the stage on the red side of the spectrograph which carries the bundles for  $\lambda 525.0$  nm and  $\lambda 676.8$  nm.

In order to eliminate the arbitrary velocity offset between the two systems we use an average profile for the MWO pixels with a center-to-limb angle of  $3^\circ$  or less as the velocity zero reference for the image. We refer to these pixels as the disk center pixels. The observed solar line for Ni I multiplet 57 with a laboratory wavelength of  $\lambda 676.78$  nm is a good reference because the MDI Lyot filter is quoted by Scherrer et al. (1995) as having its peak  $45$  mÅ redward of the mean solar wavelength. We do not attempt to trace wavelengths back to a laboratory standard but instead use the disk center solar line as our reference wavelength. The only wavelength standard we require is that which establishes the relationship between our fiber-optic pickups and the position of the MDI filters. Consequently, the observed position of the mean solar line can function as the connecting intermediary without regard to its absolute position since it can be measured by both MWO and MDI. This procedure fixes the relative position of our observed line profiles and the maximum of the MDI Lyot filter. The phasing of the MDI Michelson filter tunings is then found from the MDI integrated absolute velocities as reported by the LOI summaries. We adjust our model of the Michelson filters until the disk center velocity reproduces the LOI velocity. We should also include the limb shift function since the LOI integration covers most of the solar disk. However, this additional effect is small compared to those we do include and the included effects do not significantly alter the magnetic field determination. Consequently, our approach is adequate for the purpose of reproducing the magnetic fields.

To obtain the magnetic field in each pixel, we reconstruct both LCP and RCP NiI line profiles at the velocity offset of MDI using the 10-point measurements from the two polarization phases. We set a lower limit for the intensity used in the analysis to eliminate the outermost part of the solar limb where the line profiles are highly distorted. The very high magnetic field in the sunspot areas will be dropped from the comparison later by superimposing the intensity image on top of the magnetic image to locate the sunspots' positions. The left (right) continuum level of each line profile is set equal to the leftmost (rightmost) of the 10 points, and the core of the profile is reconstructed using a spline fit over the 10 points. We use these line profiles the same way SOHO/MDI does on board to compute the Doppler signal (Scherrer et al. 1995). From the difference  $\Delta v$  between two velocities we calculate the magnetic strength  $\Delta B$  of that pixel using the formula:

$$\frac{\Delta v}{\Delta B} = 1.42225 \quad \text{m/s/Gauss} \quad (1)$$

We adopted the spline fit instead of the Lorentzian fit for the intensity profiles because the spline method is able to accommodate a wider variety of variations which in practice caused the Lorentzian method to fail for many profiles, especially those near the limb and in sunspots. Moreover, if the line

can be properly fitted with the Lorentzian wings, the differences in the continuum levels between two approaches are less than 3.5%, resulting in the difference less than about 6.0% in the calculated magnetic strength. Finally, the raw MWO magnetogram is interpolated into a 512 by 512 pixel image. This image is the proxy MDI. The non-interpolated MWO NiI  $\lambda 676.8$  nm magnetograms will be compared directly to the MWO FeI  $\lambda 525.0$  nm magnetograms later.

We summarize here the explicit steps in the creation of the proxy MDI magnetogram from MWO data:

1. We take the average of the 10 pickup positions to be the position of the stage as a whole.
2. Using the spectrograph dispersion and the pickup positions we find the wavelength offset for each pickup relative to the stage position which we define to be an array:  $X_{\text{arr}}$  having units of mÅ. Figure 1 gives the wavelength offset array along its top axis.
3. We select as the disk center pixels all those which have a center-to-limb angle less than  $3^\circ$ . We then find the average servo position for the disk center pixels and determine the offset of each pixel from the average. We convert the stage position difference, pixel - average, to a wavelength offset  $d\lambda$  which is then added to  $X_{\text{arr}}$  to give the servo corrected position of each pickup for each pixel. We subtract the average of the servo shifts for all the disk center pixels from the individual pixel's servo position and divide the difference by the spectrograph dispersion to obtain the pixel's wavelength offset, called  $d\lambda$ , in mÅ. Adding  $d\lambda$  to  $X_{\text{arr}}$  gives the servo-corrected locations of each pickup in each pixel. For the purpose of obtaining a reference line profile we average the intensities of the two states of circular polarization, RCP and LCP, to obtain the average intensity  $I_{\text{avg}}$ .
4. Using spline interpolation we calculate  $I_{\text{new}}(X_{\text{arr}})$  from  $I_{\text{avg}}(X_{\text{arr}} + d\lambda)$  for each of the disk center pixels. The intensities for the disk-center pixels are thus brought to a common wavelength basis. Figure 2 demonstrates the servo correction and interpolation steps.
5. We average the  $I_{\text{new}}$  of the disk center pixels to have one reference 10-point line profile.
6. We over sample this line profile using spline interpolation near the core and a Lorentzian fit in the wings to reconstruct the complete line profile at the center of the solar disk. The shift of the bottom of the line from the center of the pickup set is calculated using the bisector method. We call this shift  $dx$ .
7. We use ephemeris formulae to compute the relative Sun-Earth orbital and rotation velocities from the Mt. Wilson site at the observed time of the pixel at the center of the solar disk, and convert the total velocity to the Doppler shift, called  $dl$ . Subtracting  $dx$  from  $X_{\text{arr}}$  corrects the MWO pickups' locations for the servo, while adding  $dl$  to  $X_{\text{arr}}$  corrects the line profile at the center of the solar disk for the Earth's rotation and orbital motions. Therefore the plot of the complete line profile vs.  $(X_{\text{arr}} - dx + dl)$  is what would be seen by MDI. Figure 3 shows

the fitted MWO NiI  $\lambda 676.8$  nm line profile at the solar disk center on 20 Aug, 2000 at 19:24 UT. The plot shows the average of the disk center pixels with the zero point of the profile taken to be the minimum wavelength. The arrow shows the position of the initial reference point which is the average of all the pickup positions.

8. The profile is shifted to account for the Sun-spacecraft velocity of SOHO, the MDI filters are simulated and convolved over this disk center line profile.
9. The phase of the MDI Michelson filter system is adjusted so that it reproduces the velocity offset determined from the LOI data from MDI.
10. Applying the central pixel shifts to the rest of the image, we build up an array of line profiles, each of which is at the wavelength position where it is observed by MDI.
11. Finally, model MDI filter functions are applied to the observed line profiles for both states of circular polarization in order to determine the velocity difference between these states and thus the magnetic field. Figure 4 is one example of how  $\Delta B$  is calculated from MWO data.

### 3.2. Create Proxy MWO from MDI Magnetograms

From the given coordinates and observed time of each pixel in the MWO data, we select the corresponding pixels in the MDI magnetograms. If the MWO observed time is in between two MDI images, then we perform a linear interpolation on the corresponding MDI pixels. The magnetic field strengths of these MDI pixels are then averaged to obtain the equivalent magnetic field of one MWO pixel. Interpolating the resulting irregular array into a 512 by 512 pixel frame gives a proxy MWO created from MDI magnetograms.

### 3.3. Create MWO FeI $\lambda 525.0$ nm Magnetograms

As described by Howard et al. (1983), there are 4 quantities obtained from the MWO FeI  $\lambda 525.0$  nm observation:  $A_1$ ,  $B_1$ ,  $A_2$ , and  $B_2$ .  $A_1$  and  $A_2$  are the integrated intensities of slit A at phases 1 and 2, and  $B_1$  and  $B_2$  are the integrated intensities of slit B at phases 1 and 2. From these quantities, we calculate the magnetic signal  $Z = A_1 - B_1 - A_2 + B_2$  and the total intensity  $I = A_1 + B_1 + A_2 + B_2$  in each MWO pixel, and compute the image's  $Z/I$  histogram to find the bias  $ZOIB$ , which is the value of the most occurrences of  $Z/I$  in this image. Next, using the calibration linescans, we calculate the total error

$$E_c = A_{1c} - B_{1c} + A_{2c} - B_{2c} \quad (2)$$

as a function of the pickups' positions (in microns), where c denotes the calibration state. We then fit the micron ( $Y_c$ ) vs  $X_c = E_c/I_c$  by a function

$$Y_c = aX_c + bX_c^2 + cX_c^5 \quad (3)$$

to find the coefficients  $a$ ,  $b$ , and  $c$ . After that, in each pixel, we compute phase 1 error over intensity  $X_1$  and phase 2 error over intensity  $X_2$ , where

$$X_i = \frac{2(A_i - B_i)}{I} + (-1)^i ZOIB \quad (i = 1, 2) \quad (4)$$

For each  $X_i$ , there is an equivalent shift of the line profile  $Y_i$  in microns given by

$$Y_i = aX_i + bX_i^2 + cX_i^5 + [1 - \cos \rho](576.4066X_i + 114.6506X_i^2 + 29628.58X_i^5) \quad (i = 1, 2) \quad (5)$$

The last term is the center-to-limb-magnetic-strength correction with  $\rho$  being the center-to-limb angle. The magnetic strength of that pixel,  $B_{5250}$ , can be deduced from the difference  $\Delta Y = Y_1 - Y_2$  and from the following equation:

$$B_{5250} = \frac{\Delta Y \times SaF}{DP \times CF} \quad (6)$$

where  $DP = 15219.271\mu \text{ \AA}$  is the MWO spectrograph dispersion,

$$CF = 2 \times 4.67 \times 10^{-13} g(5250.2)^2$$

is the conversion factor, the effective  $g$  factor is 3 and  $SaF = (4.5 - 2.5 \times (1 - \cos^2(\rho)))$  is the saturation factor.

A MWO FeI  $\lambda 525.0$  nm magnetograms is obtained after all pixels are computed.

## 4. Alignment and Comparison

### 4.1. Proxy MWO vs Proxy MDI

To reduce the discrepancy between the proxy images due to the difference in spatial resolution, we apply a Gaussian filter with FWHM = 4 pixels to the magnetograms. After that, we align these proxy images by rotating the proxy MWO about its center and shifting in x and y directions to get the highest correlation between two magnetograms in the region with the center-to-limb spherical angle  $\rho \leq 60^\circ$ . This step is important because the solar poles and the solar centers in the original magnetograms do not coincide. The amount of shift and rotation required to obtain the maximum correlation is shown in figure 5 for the images used in this work. In most cases the rotation angle required is less than 0.5 degrees and the maximum shift is about 1 pixel and mostly along the y (North-South) direction. The images are then divided into rings with  $(\rho_{min}, \rho_{max})$  are  $(0^\circ, 30^\circ)$ ,  $(30^\circ, 45^\circ)$ ,  $(45^\circ, 60^\circ)$ , and  $(60^\circ, 85^\circ)$ . The last two rings are further separated into Northwest, Northeast, Southeast, and Southwest. This separation can be seen in figure 6. To increase the signal-to-noise ratio and to reduce the system's errors, we group about one month of data together. Each group contains at most one image per day with observation time between 18:00 UT and 22:00 UT. In addition, because MWO equipment is not optimized to detect very high magnetic field, we

only select zones with absolute magnetic strength less than 400 Gauss for the comparison. The corresponding regions of two sets of data are then fit linearly to obtain the slope of proxy MWO vs proxy MDI  $a_1$  and the slope of proxy MDI vs proxy MWO  $a_2$ . The scale factor  $sf_1$ , which is the factor that multiplied the proxy MWO to get the proxy MDI, is just

$$sf_1 = \frac{1}{2} \left( \frac{1}{a_1} + a_2 \right) \quad (7)$$

A comparison between NiI  $\lambda 676.8$  nm full-disk magnetograms from the MDI instrument and the Advanced Stokes Polarimeter to rescale the MDI magnetograms has been recently published by Berger & Lites (2003). Our work however covers a much larger area of the solar disk, and includes both magnetic and quiet regions. In Berger & Lites (2003) the comparison was done for only one day of observations while our work extends this comparison to several years of data.

#### 4.2. Proxy MDI vs MWO FeI $\lambda 525.0$ nm Magnetograms

The same set of the MWO FeI  $\lambda 525.0$  nm as the MWO NiI  $\lambda 676.8$  nm is selected to compare to the raw MWO NiI  $\lambda 676.8$  nm. The alignment is not needed because these lines are observed simultaneously by the same method. We separate each image into 10 regions and group the magnetograms exactly the same way as the comparison between proxy MWO and proxy MDI. We then use the same fitting method to obtain the scale factor  $sf_2$  that multiplies the MWO FeI  $\lambda 525.0$  nm to get the raw MWO NiI  $\lambda 676.8$  nm.

Finally, we calculate the scale factor for each region on the solar disk

$$sf = \frac{sf_1}{sf_2} = \frac{\text{MWO FeI } \lambda 525.0 \text{ nm}}{\text{MDI}} \quad (8)$$

### 5. Results

We are interested in determining the time dependence of the relationship between the MDI and MWO measured magnetic fields over intervals of weeks to years. The passage of active regions across the solar image affects our ability to determine the scale factors since the method we use is most effective when plage regions of moderate field strength are present. The spectral lines are greatly modified inside sunspots and make the use of both MWO and MDI algorithms of doubtful validity for these regions. In order to obtain a stable and valid relationship between the two systems, we use scatter diagrams which collect measurements from images obtained over periods close to the equatorial rotation period. We also choose the time intervals so that the averaged images do not span the times when the MDI filter system was retuned. In this way any effect of the retuning can show up as a jump in the derived scale factors. We also provide in table 3 the global averaged scale factors that represent our best estimate of the relationship between the two data

sets. The errors given in tables 1 to 3 are the rms deviations from the averages of the individual data periods discussed below and are not based on the formal errors of determination for each of the points plotted in figures 7 to 9. Leading up to table 3 are two preliminary results giving in table 1 the scale factors between two methods of measuring the magnetic strength both using the same line  $\lambda 676.8$  nm and in table 2 the scale factor for the relationship between two different lines  $\lambda 525.0$  nm and  $\lambda 676.8$  nm using the same MWO method. Note that for both table 2 and table 3 the magnetic fields for the  $\lambda 525.0$  nm case have been corrected from the raw observational values by multiplication by the saturation factor. The quantities plotted in figure 6 are from table 3.

As an indication of the quality of our ability to create images that are closely similar to each other we show in figure 10 an example of a pair of MWO and MDI proxy images taken on August 20, 2000. Image a is created from MWO observations and image b is from the MDI magnetograms. One can see that the stronger-field features are well correlated across the two images. The thin, black ring surrounds the proxy MDI is the region where the intensities fall below the accepted low limit, which is 5% of the images's maximum intensity. This region will be excluded from the MDI-MWO comparison. Image c is obtained by subtracting image b from image a. Image d is obtained by multiplying image b to the derived scale factors in table 1 and subtracting the result from image a. The residual features visible in image d are mainly due to two factors. First, only pixels with an absolute magnetic field value less than 400 Gauss are included in the calculation of the scale factor, so features with greater magnetic field values will not be properly rescaled. Second, the scale factor applied to image b is the average value obtained from all observations, and may be slightly different from the one calculated for that particular case.

Figure 11 shows the scatter plots of the proxy images in figures 10a and 10b. Each plot is for a different region on the solar image as indicated. In each plot, there are two linear fits: one is for proxy MWO vs proxy MDI and the other is for proxy MDI vs proxy MWO. The former fit is drawn directly (the dotted line), whereas the dashed line is the reversed ( $x$  to  $y$  and  $y$  to  $x$ ) of the latter fit. The scale factor and the cross-correlation of each plot are shown along with the equations of the two lines. Figure 10 shows clearly that in these selected magnetograms, the west-side part of the image contains much more magnetic features than the east-side. That causes the west-side correlations to be higher than the corresponding east-side correlations. To overcome the uneven distribution of the magnetic features in any particular image, we group about one month of magnetograms before doing the comparison as mentioned in section 4.1.

Figure 12 shows the scatter plots of the groups of magnetograms from August 6, 2000 to August 26, 2000, which includes the images in figure 10. The format here is the same as in figure 11. One can see that with the grouping technique, the correlations between different regions are now about the same. Furthermore, the correlations above 0.9 indicate that these data sets are well correlated. The very small error associated with some of the scale factors is the result of the very large number of points used in that particular fit. As an example, the (0,30) region in figure 12 contains more than 500,000 pairs of points. The shutter noise has been shown to induce a small random shift of the zero point in full-disk magnetograms obtained by MDI (Liu et al. 2004). Figure 13 shows the

sensitivity of the scale factor to the zero point shift detected in full-disk magnetograms obtained by MDI. The results shown on the left plots were obtained without any correction for this offset, while the right plots show the value of the scale factor calculated by correcting for this effect. The offset does not produce any significant effect on the calculated scale factor.

Figures 7, 8, and 9 show the plots of the scale factors  $sf_1$  (proxy MDI/proxy MWO),  $sf_2$  (raw proxy MDI/MWO FeI  $\lambda 525.0$  nm), and  $sf$  (MWO FeI  $\lambda 525.0$  nm / MDI) vs time for 10 regions. Figure 9 also shows the scale factor obtained from a direct calculation using MWO FeI  $\lambda 525.0$  nm magnetograms. As discussed in section 2.0, this approach is likely to produce a bias due to the non-calibration of the MWO 6768 spectral line used in this work. From the analysis of figure 9 we see that this bias is particularly evident near the solar limb. In each plot, the vertical dashed lines indicate when the MDI tuning changes occurred, and the horizontal dashed line is the average of the scale factors. Note the different vertical scales of these plots. The error bars shown in these plots are  $3\sigma$ . There are interesting results that we can extract from these figures. First, there had been little change in the MDI magnetograms due to the SOHO/MDI tuning changes. One can see that from the variations of  $sf_1$  and  $sf$  in the center regions ( $\rho \leq 45^\circ$ ). Secondly,  $sf_2$  increases from the center (0.47) to the limb (0.54), whereas  $sf$  decreases from the center (1.82) to the limb (around 1.60). Finally, there are jumps in  $sf_1$  and  $sf$  between the east-side and the west-side with  $\rho \geq 45^\circ$ . Possible causes for these effects are discussed in the next section.

The important point here is the averaged scale factors of 1.70 to 1.89 between the MWO FeI  $\lambda 525.0$  nm magnetograms and the MDI magnetograms. As shown in Evans (1999, figure 2.6), the spectral lines NiI  $\lambda 676.8$  nm and FeI  $\lambda 525.0$  nm are formed at roughly the same height in the solar atmosphere, which is about 350 km above  $\tau_{5000} = 1$ . Therefore, these ratios are properly due to the saturation factor applied to the MWO FeI  $\lambda 525.0$  nm magnetograms as shown in equation (6). This result is very close to the previous results shown in Ulrich et al. (2002, table 2) for the inner regions on the solar disk. The table implies that the ratio between MWO FeI  $\lambda 525.0$  nm magnetograms with the saturation factors applied and the MWO method magnetogram for  $\lambda 676.8$  nm  $\pm 2.8$  pm will be 1.6 to 1.7 for  $\rho \leq 30^\circ$ , 1.5 for  $30^\circ \leq \rho \leq 45^\circ$ , and 1.2 for  $45^\circ \leq \rho \leq 70^\circ$ . Table 2 in this paper shows the corresponding values are 2.1, 2.0, and 1.9. The near-the-limb discrepancy between the two results may come from the fact that the number of images used before was limited and may not be statistically significant. In general, the difference between the magnetic field measured with different spectral lines is a complicate matter that depends on a combination between the particular model for the structure of the magnetic flux tubes and the line formation process. Such analysis is beyond the scope of this paper, but some details are given in Ulrich et al. (2002).

## 6. Conclusion

The results discussed in the previous section indicate that the current Level 1.8 MDI full-disk solar magnetogram gauss levels are systematically lower than the MWO FeI  $\lambda 525.0$  nm by a factor of about 1.7. The analysis also shows that while this scale factor is quite stable over the period

of time investigated in this paper, it does show a slight dependence on the center-to-limb angle. In addition, the difference in the scale factors between the west-side and the east-side implies a distortion in the MDI magnetograms relative to the MWO magnetograms. This difference may come from the angle dependence of the Michelson filters in the MDI instrument. An additional contribution may come from scattered light. As shown by Albregtsen & Andersen (1985), the straylight will cause the spectrum of any point on the solar disk to be contaminated by a weighted sum of Doppler-shifted spectra from its surroundings. For a spectral line, the combination of scattered light and limb darkening will generally produce a non-symmetrical east-west effect. In the comparison between MWO676.8 and MDI676.8 (Table 1), since the spectral line is the same, the asymmetry is introduced by the different amount of scattered light between the two instruments and observational techniques. It is interesting that also for the case shown in Table 2 there is a significant asymmetry between the east and the west sides. In this case, since the instrument is the same, the effect is likely produced by the different center-to-limb function of the two spectral lines.

With the addition of the new 24-channel data-taking system, we have established the MWO FeI  $\lambda 525.0$  nm magnetogram - MDI magnetogram relationship using data from March 1997 to August 2000. This relationship can be used to correct for the center-to-limb dependence in the MDI magnetograms. Moreover, it infers the equivalence of the two types of magnetograms. From that, one can use the MWO FeI  $\lambda 525.0$  nm magnetograms, which covers a period from 1967 to the current time, to study the variation in the solar magnetic field and the effect of this variation in the near-Earth space environment, and to test the solar dynamo theories. As a result, it is possible to predict a near future solar magnetic field. There are several factors that may affect the results of the calibration.

1. The MWO magnetograms measure the magnetic field using the longitudinal component of the Zeeman effect which causes the line wings to be circularly polarized. The coelostat system at the 150-foot tower modifies the measured magnetic field due to the oblique reflections by two mirrors which partially depolarize the radiation. Even though we have chosen the MWO observed time around local noon, the solar declination still leads to some differences between the calculated MWO summer magnetograms and MWO winter magnetograms. The Earth's atmosphere, in addition, is another factor that affects the MWO observation. The time scale of 25 minutes to complete one fastgram (40 minutes for one slowgram) is long enough for the atmosphere to change its condition. However, because of the scanning method used at Mt. Wilson, this factor is not the cause of the east-west discrepancy in the scale factor  $sf$ . This can only lead to some differences between the North and the South in the MWO magnetograms.
2. The differences in spatial resolution and observed time between the MDI magnetograms and the MWO magnetograms require several interpolating steps before the comparison as described in section 3. These steps may generate some error in the analyses.
3. As described by Ulrich et al. (2002), the solar magnetic field in excess of 200 Gauss will result in the saturation in the MWO FeI  $\lambda 525.0$  nm calculated magnetic field. The saturation

factor applied in the equation (6) above may cause some error at the high ends of the MWO  $\lambda 525.0$  nm magnetograms.

4. The definition of the radius is different between MDI and MWO partly due to the smaller pixels for MDI and partly due to the different distance to the sun.

This work has been supported by grants from NASA and Stanford University. We thank John Boyden and Rick Bogart for their very helpful suggestions.

## REFERENCES

- Albregtsen, F. & Andersen, B.N. 1985, *Sol. Phys.*, 95, 239
- Altschuler, M. D. & Newkirk, G. 1969, *Sol. Phys.*, 9, 131
- Arge, C. N., Hildner, E., Pizzo, V. J., & Harvey, J. W. 2002, *Journal Geophysical Research (Space Physics)*, 16
- Arge, C. N., Odstrcil, D., Pizzo, V. J., & Mayer, L. R. 2003, in *American Institute of Physics Conference Series*, 190–193
- Arge, C. N. & Pizzo, V. J. 2000, *J. Geophys. Res.*, 105, 10465
- Berger, T.E. & Lites, B.W. 2003, *Sol. Phys.*, 213, 213
- Evans, S. E. 1999, Ph.D. Thesis
- Hakamada, K., Kojima, M., Tokumaru, M., Ohmi, T., Yokobe, A., & Fujiki, K. 2002, *Sol. Phys.*, 207, 173
- Howard, R., Boyden, J. E., Bruning, D. H., Clark, M. K., Crist, H. W., & Labonte, B. J. 1983, *Sol. Phys.*, 87, 195
- Lean, J. 2000a, *Geophys. Res. Lett.*, 27, 2425
- Lean, J. L. 2000b, *Space Science Reviews*, 94, 39
- Liu, Y., Zhao, X., & Hoeksema, J.T. 2004, *Sol. Phys.*, 219, 39
- Lockwood, M., Stamper, R., & Wild, M. N. 1999, *Nature*, 399, 437
- Schatten, K. H., Wilcox, J. M., & Ness, N. F. 1969, *Sol. Phys.*, 6, 442
- Scherrer, P. H., Bogart, R. S., Bush, R. I., Hoeksema, J. T., Kosovichev, A. G., Schou, J., Rosenberg, W., Springer, L., Tarbell, T. D., Title, A., Wolfson, C. J., Zayer, I., & MDI Engineering Team. 1995, *Sol. Phys.*, 162, 129

- Solanki, S. K. & Fligge, M. 2000, *Space Science Reviews*, 94, 127
- Solar and Space Physics Survey Committee. 2003, *The Sun to the Earth and Beyond: A Decadal Research Strategy in Solar and Space Physics* (Washington, D.C.: The National Academies Press)
- Ulrich, R. K., Evans, S., Boyden, J. E., & Webster, L. 2002, *ApJS*, 139, 259
- Wang, Y.-M., Lean, J., & Sheeley, N. R. 2002, *ApJ*, 577, L53
- Wang, Y.-M. & Sheeley, N. R. 1990a, *ApJ*, 365, 372
- . 1990b, *ApJ*, 355, 726
- . 1992, *ApJ*, 392, 310
- Wang, Y.-M., Sheeley, N. R., & Nash, A. G. 1991, *ApJ*, 383, 431

Table 1: The scale factor for  $\lambda 676.8$  nm due to two different magnetic field measurement methods

MWO676.8 / MDI676.8		
REGION	RATIO	$\sigma$
(0,30)	0.854	0.019
(30,45)	0.900	0.019
(45,60)NE	0.929	0.031
(45,60)NW	0.904	0.030
(45,60)SE	0.946	0.031
(45,60)SW	0.938	0.034
(60,85)NE	0.971	0.046
(60,85)NW	0.914	0.034
(60,85)SE	0.995	0.048
(60,85)SW	0.955	0.045

Table 2: The scale factor between two different lines:  $\lambda 676.8$  nm and  $\lambda 525.0$  nm using the MWO method of magnetic field determination.

MWO676.8 / MWO525.0		
REGION	RATIO	$\sigma$
(0,30)	0.470	0.008
(30,45)	0.488	0.009
(45,60)NE	0.490	0.013
(45,60)NW	0.514	0.012
(45,60)SE	0.491	0.009
(45,60)SW	0.515	0.013
(60,85)NE	0.518	0.024
(60,85)NW	0.535	0.019
(60,85)SE	0.516	0.021
(60,85)SW	0.537	0.018

Table 3: The net scale factor relating the MDI magnetograms to the magnetic fields measured by the MWO synoptic program utilizing  $\lambda 525.0$  nm.

MWO525.0 / MDI676.8		
REGION	RATIO	$\sigma$
(0,30)	1.808	0.034
(30,45)	1.825	0.027
(45,60)NE	1.872	0.034
(45,60)NW	1.739	0.044
(45,60)SE	1.887	0.043
(45,60)SW	1.785	0.043
(60,85)NE	1.796	0.056
(60,85)NW	1.640	0.064
(60,85)SE	1.829	0.056
(60,85)SW	1.707	0.069

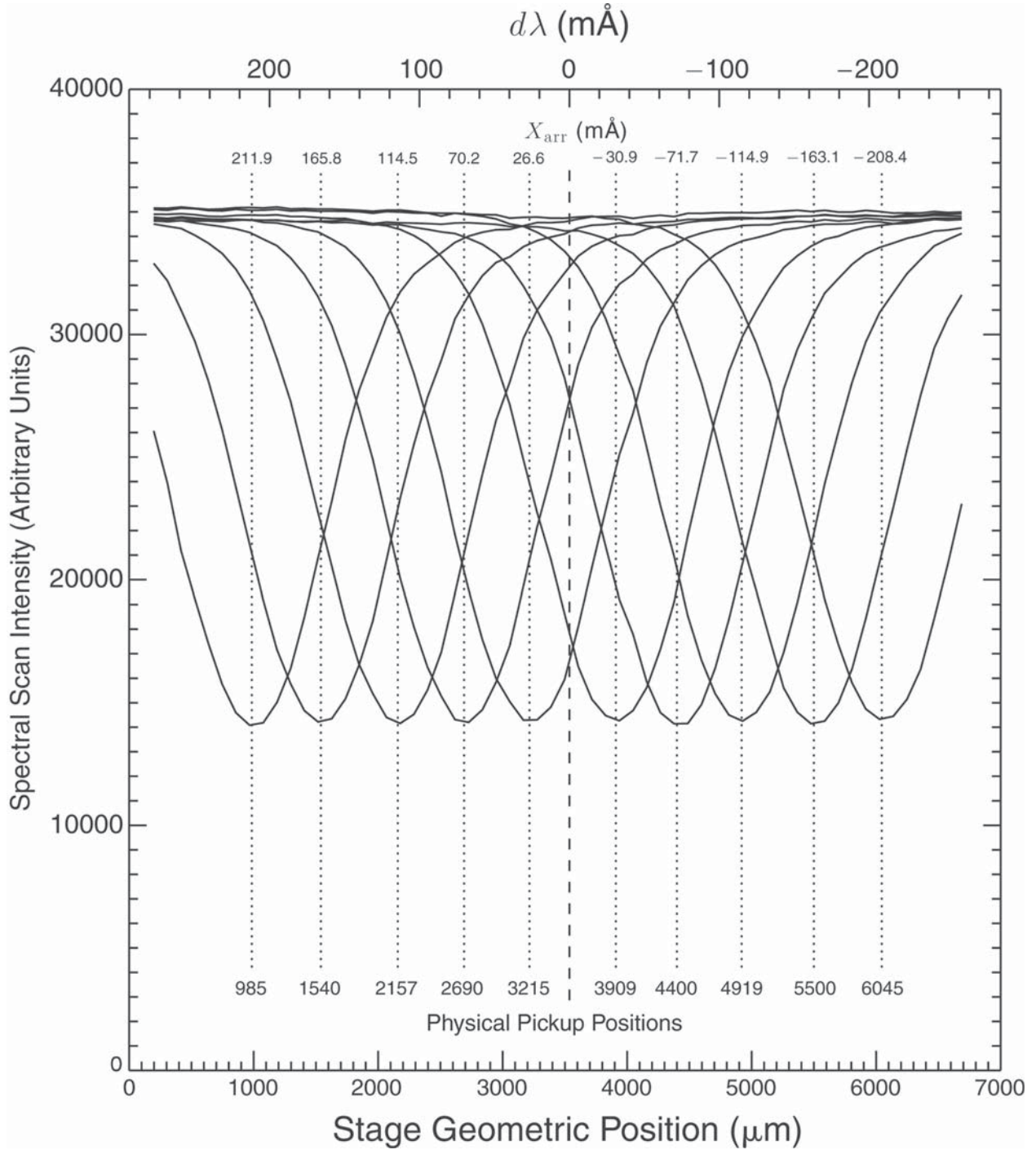


Fig. 1.— Calibration linescans for the 10 channels for NiI on 20 Aug, 2000, 19:24 UT. These linescans were adjusted so that their shapes are nearly indistinguishable. Such a scan is done for every slowgram and every four fastgrams. The vertical scale is the intensity in MWO units. The bottom horizontal axis shows the positions of the MWO pickups, whereas the top horizontal axis shows the  $X_{arr}$ , which is described in section 3.1. The dotted lines are the pickups' locations, and the dashed line is the average of the 10 pickups.

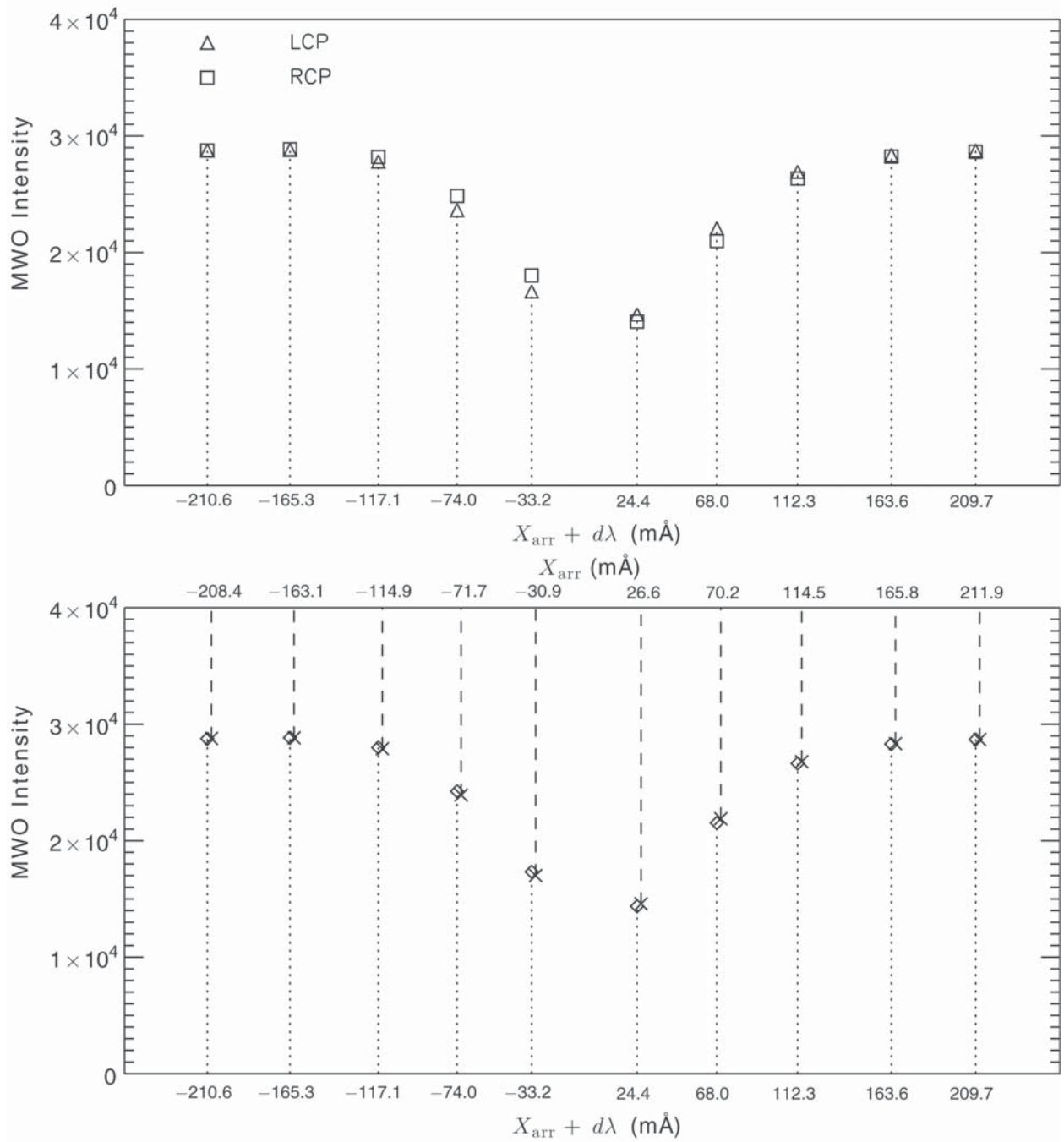


Fig. 2.— Top: a plot of data from one of the pixels in the disk center region. The vertical axis is the MWO intensity shown for the two states of circular polarization separately. The horizontal axis shows the positions of the MWO pickups plotted on the scale where the average of all positions is taken as the zero point. Before each of the disk center pixels is added to the average, the effect of its servo shift is removed by interpolation so that each pixel is treated as if the stage is in its average position. Bottom: the non-polarized intensities obtained by averaging LCP and RCP from above (diamonds) are interpolated from  $(X_{\text{arr}} + d\lambda)$  to  $X_{\text{arr}}$  (x symbols) so that the profile is referenced to the wavelength where the intensity is minimum.

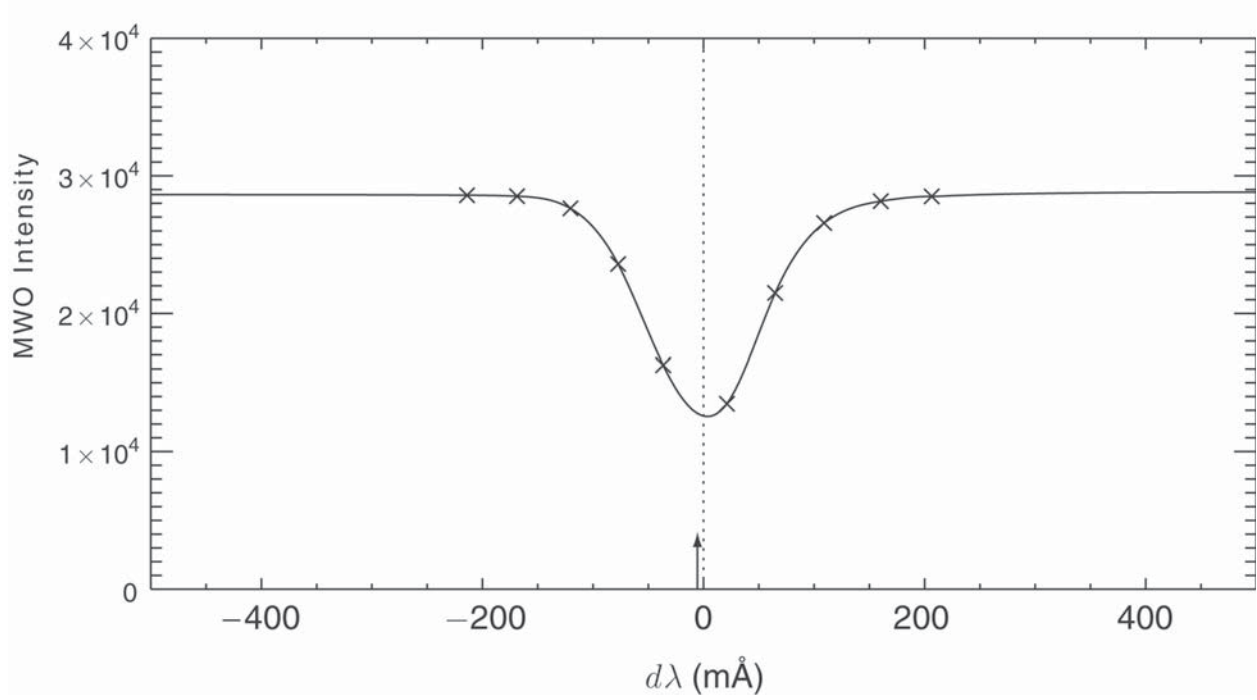


Fig. 3.— Average data of the disk center pixels after interpolation (x symbols). The solid line is the Lorentzian fit to the observed points. The position of the line center is determined using the bisector method. The initial center taken as the average position of the spectral pickups is shown by the vertical arrow. The vertical axis is the MWO intensities and the horizontal axis is the offset from the nominal reference wavelength in mÅ.

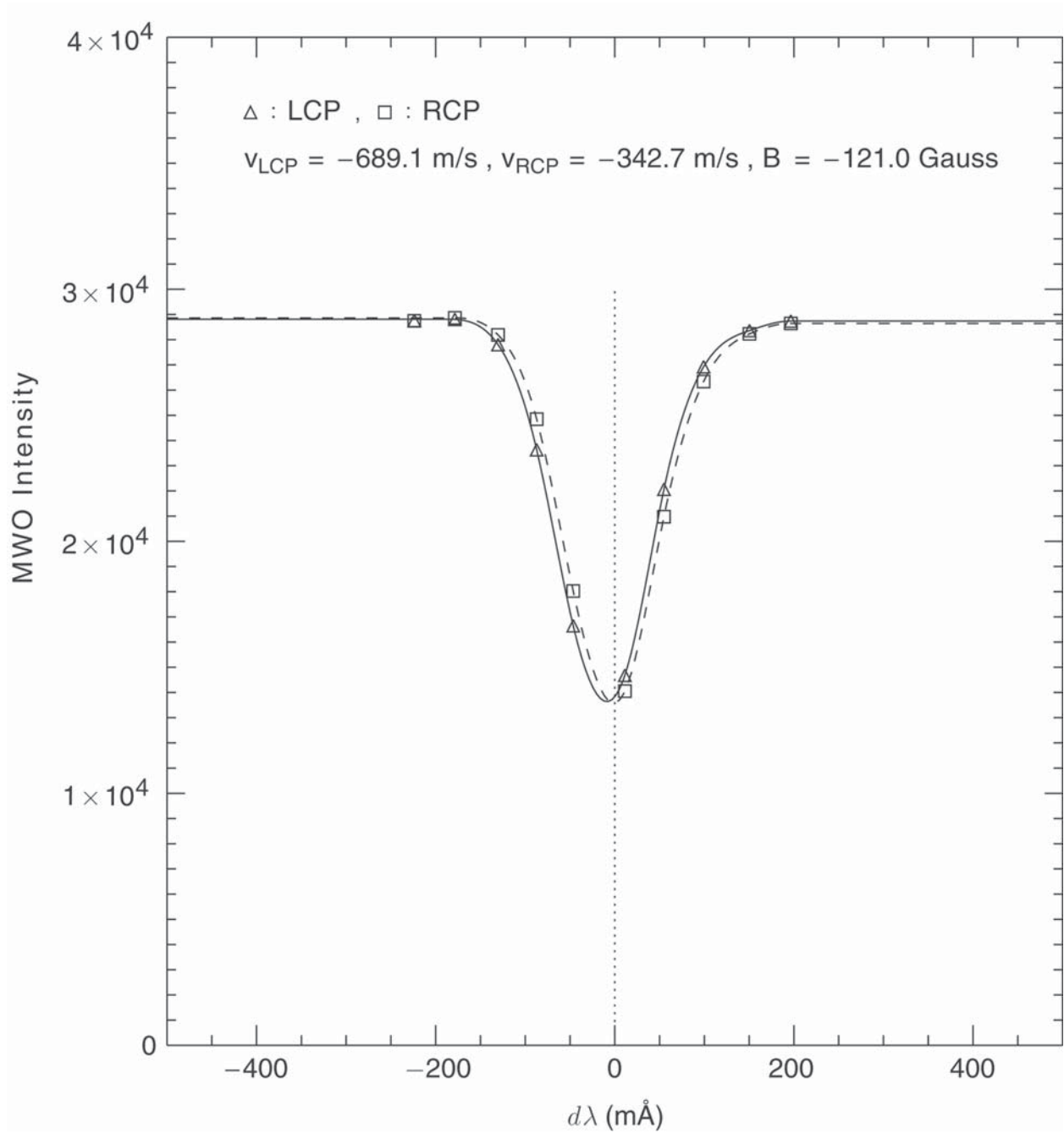


Fig. 4.— One example of a MWO pixel with a moderate magnetic field. The two states of circular polarization are shown individually. The offset velocities shown at the top of the figure have been obtained using the MDI velocity determination as described in section 3.1. The magnetic strength is then calculated from the velocity difference.

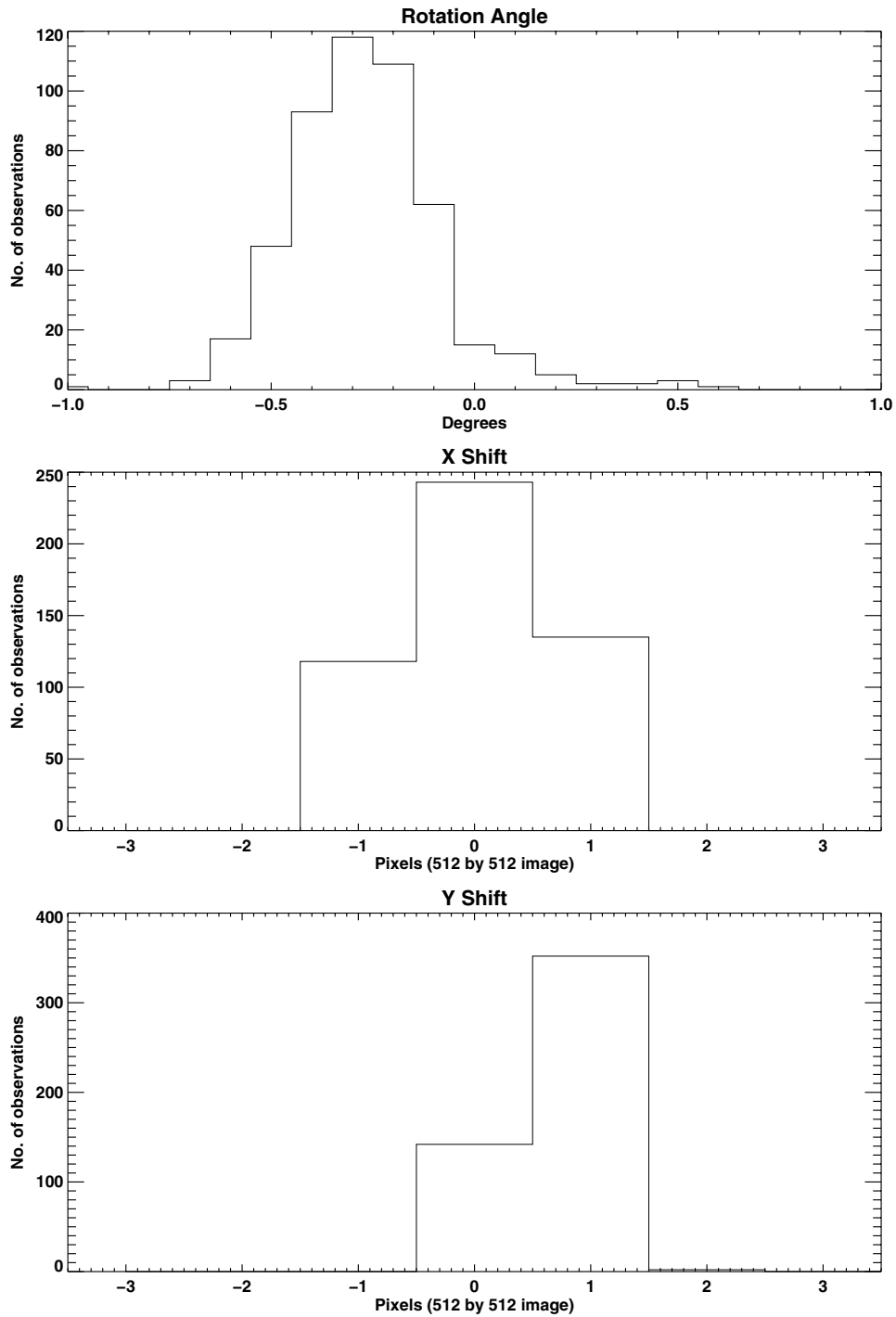


Fig. 5.— Amount of rotation (top plot), shifting in the x direction (middle plot), and shifting in the y direction (bottom plot) needed to obtain the highest correlation between the proxy MWO and proxy MDI. The histograms include all observations used for this work.

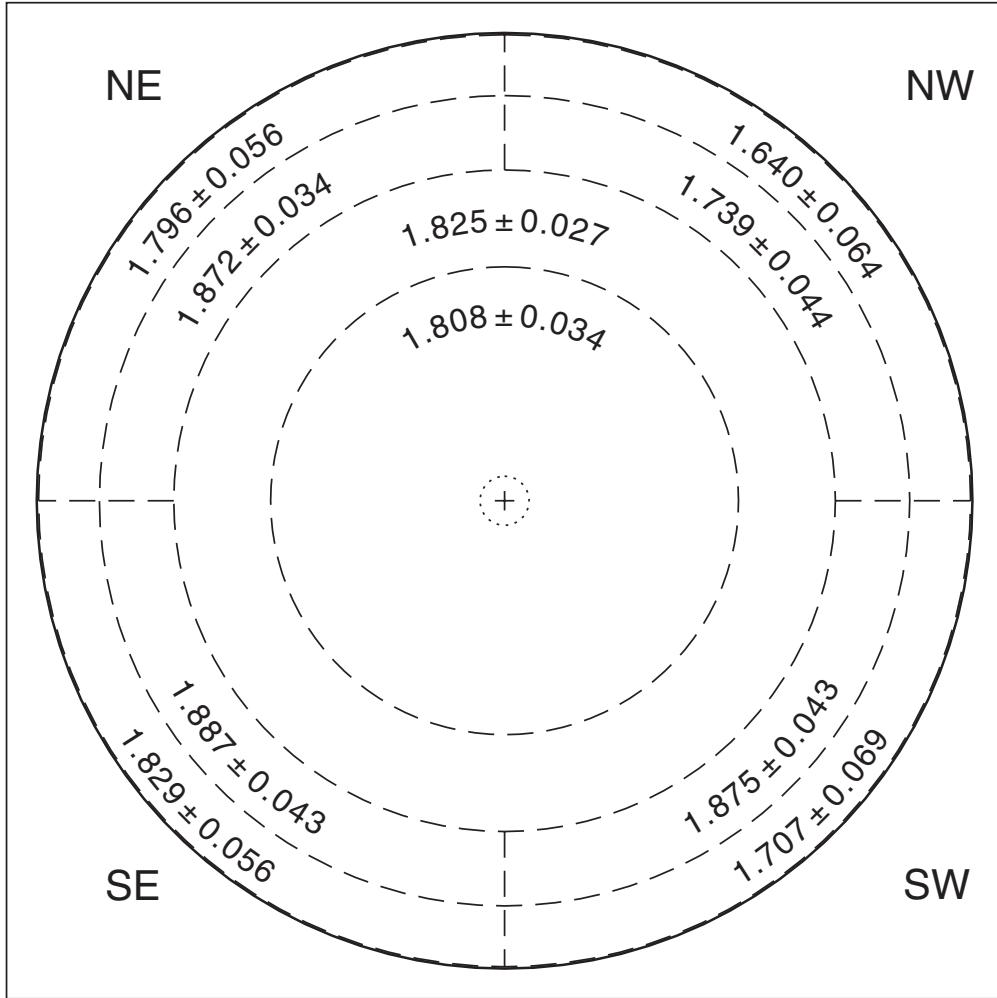


Fig. 6.— Separation of the solar disk into 10 regions as described in section 4.1. The outer circle (solid) represents the solar disk radius. Each of the sectors used for grouping is separated from the adjacent sectors by the long-dashed lines. The small circle with the short-dashed line identifies that portion of the solar disk used to define the reference wave length and the line shape calibration. The circles (from the smallest size to the biggest size) are where  $\rho = 30^\circ$ ,  $45^\circ$ ,  $60^\circ$ ,  $85^\circ$ , and  $90^\circ$ . The regions of  $(45^\circ, 60^\circ)$  and  $(60^\circ, 85^\circ)$  are further divided into Northeast, Northwest, Southwest, and Southeast.

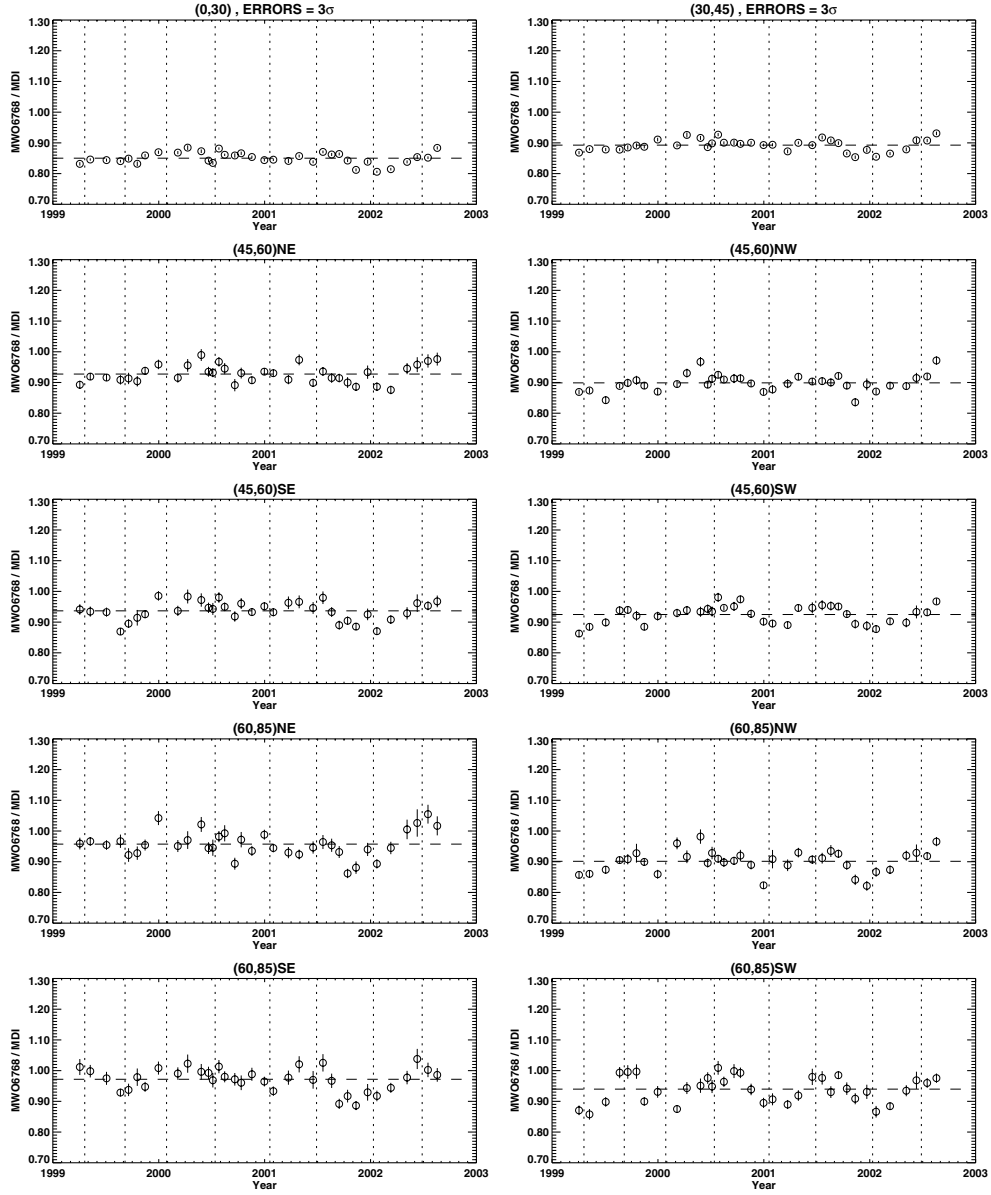


Fig. 7.— Plots of the scale factors  $sf_1$  (proxy MDI/proxy MWO) vs time for 10 regions on the solar disk. The vertical lines indicate the MDI tuning changes. The horizontal line in each plot is the average of the values in the plot. The error bars are  $3\sigma$ .

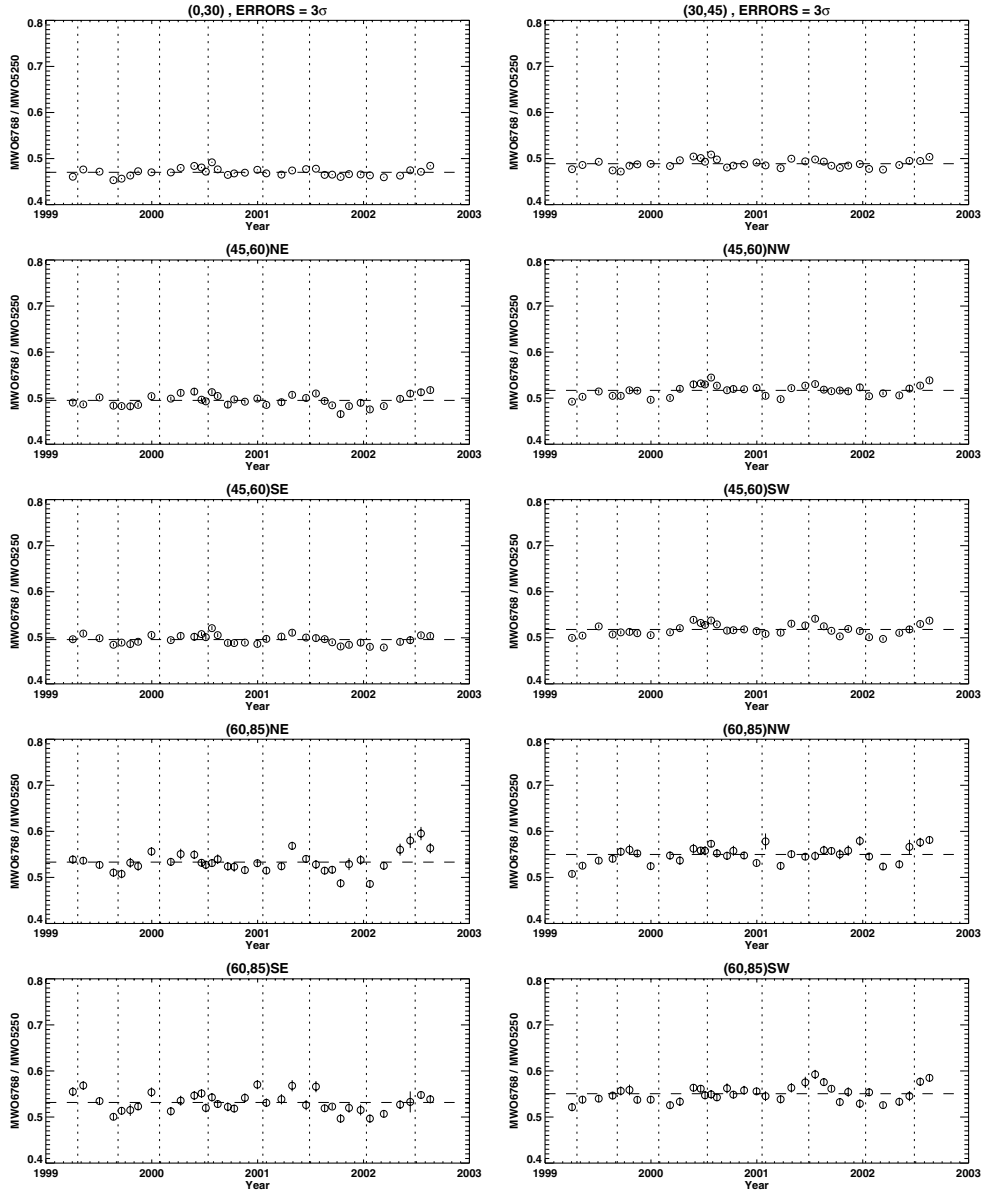


Fig. 8.— Plots of the scale factors  $s f_2$  (raw proxy MDI/MWO FeI  $\lambda 525.0$  nm) vs time for 10 regions on the solar disk. Except for the vertical scales, the format here is the same as figure 7

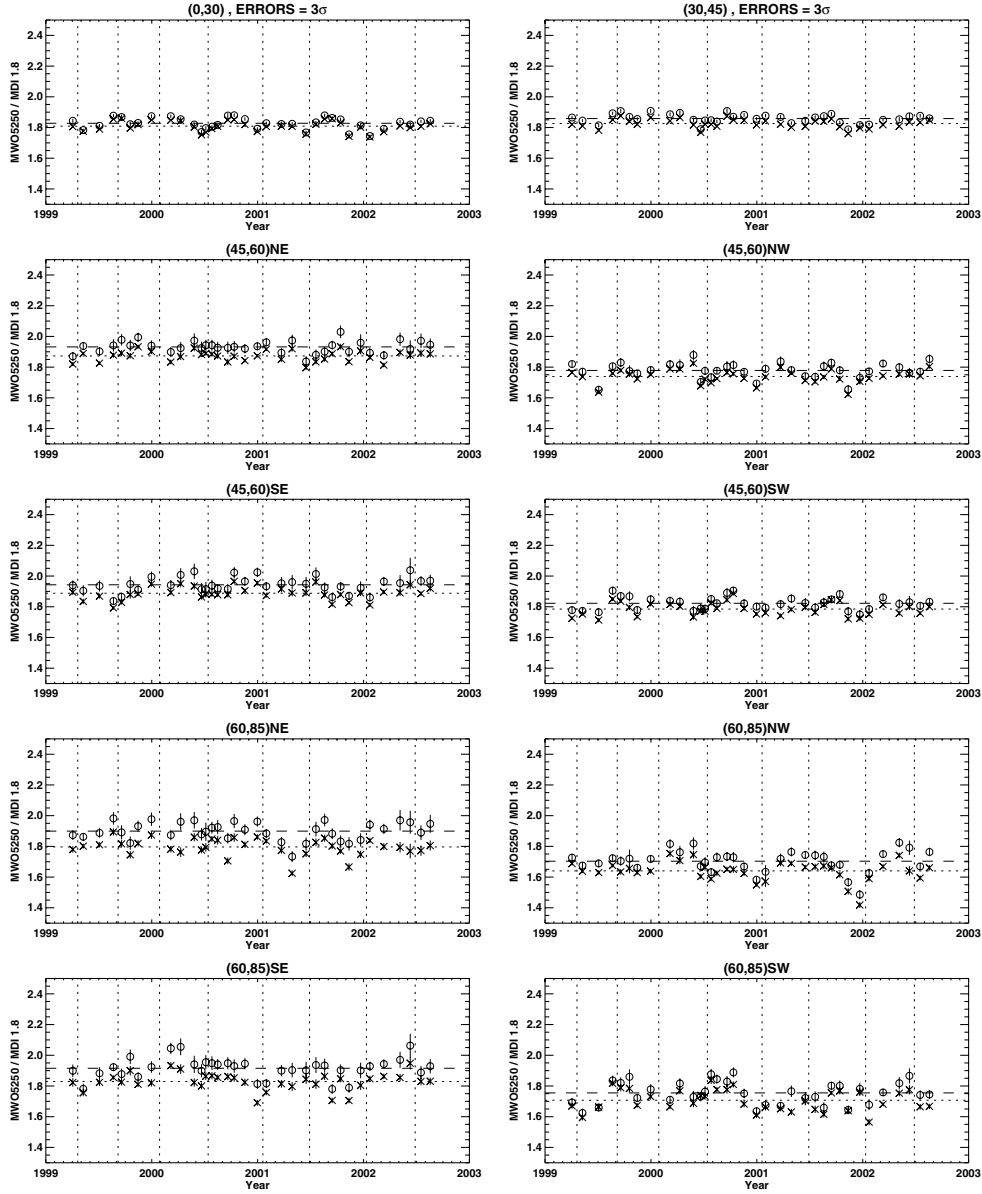


Fig. 9.— Plots of the scale factors  $sf$  (MWO FeI  $\lambda 525.0$  nm / MDI) vs time for 10 regions on the solar disk. Except for the vertical scales, the format here is the same as figure 7. The net scale factor relating the MDI magnetograms to the magnetic field measured by the MWO synoptic program is calculated using two different approaches. The circles are the results from a direct calculation using MWO FeI  $\lambda 525.0$  nm magnetograms (direct approach) while the crosses are the results from the approach followed in this paper which uses intermediary MWO NiI  $\lambda 676.8$  nm magnetograms to derive the MWO magnetic field at  $\lambda 525.0$  nm (indirect approach). The long-dash and short-dash horizontal lines in each plot are the average values of all measurements for the direct and indirect approach respectively.

OBSERVED DATE 08/20/2000

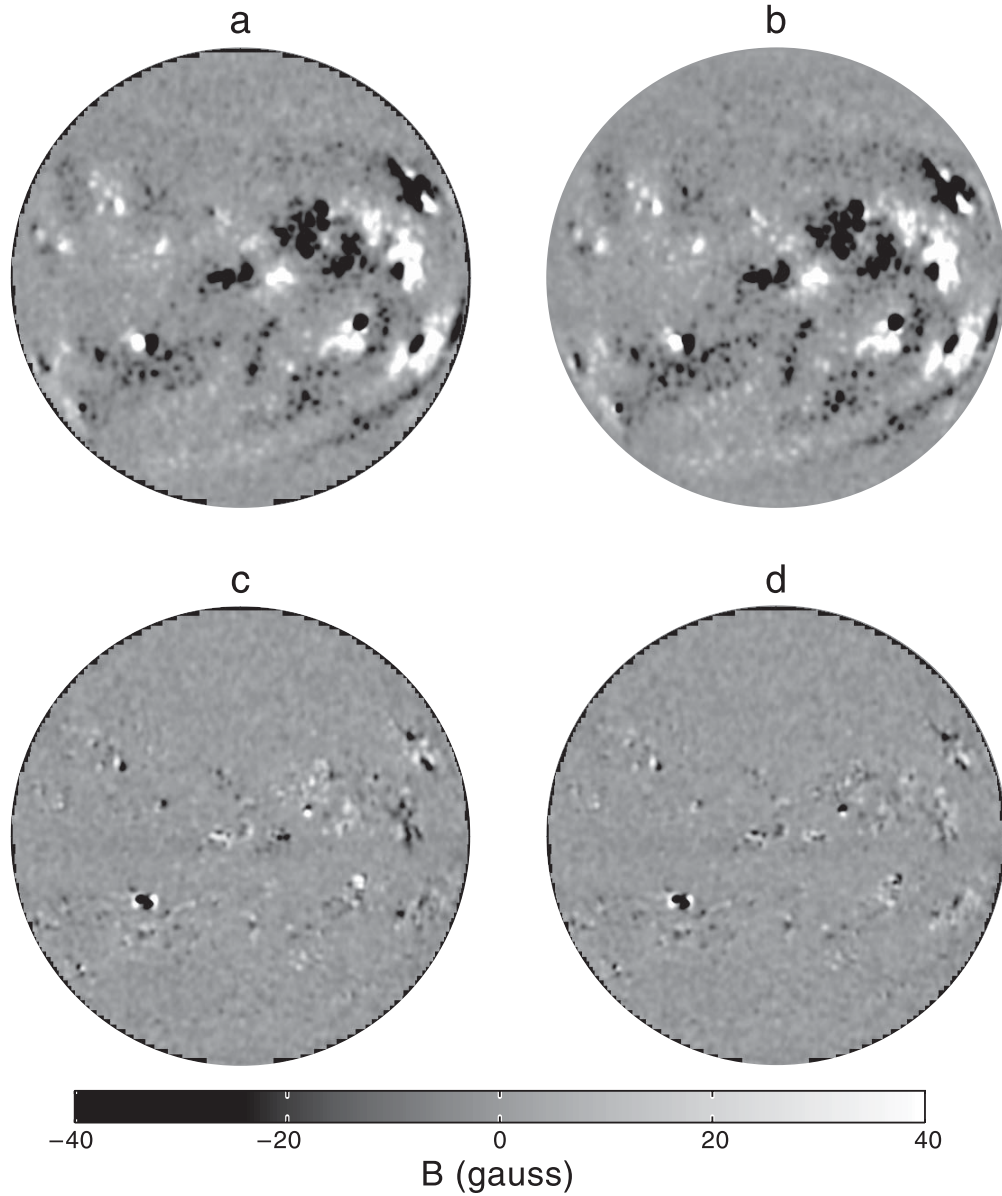


Fig. 10.— a. A simulated MDI magnetogram (calculated from MWO observation) on 20 Aug, 2000, 19:24 UT.

b. The corresponding simulated MWO magnetogram (calculated from MDI magnetograms).

c. A difference image obtained by subtracting image b from image a.

d. A difference image obtained by subtracting image b multiplied by the derived scale factors from image a. Below all four images is a greylevel bar indicating the relationship between the image darkness and the assigned magnetic field value.

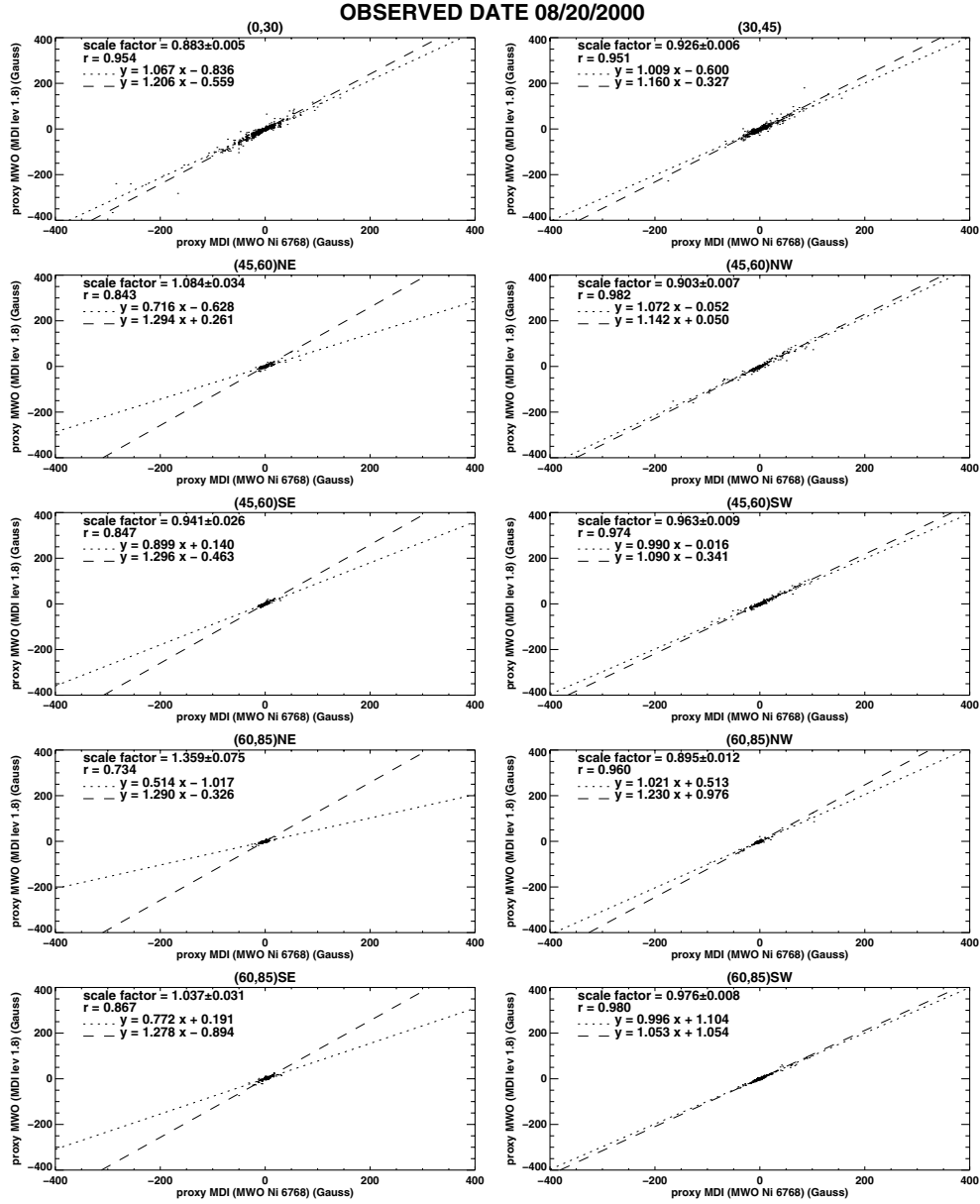


Fig. 11.— The scatter plots of the 10 regions selected from figure 10 a and b. In each plot, the dotted line is the least square fit of  $y$  vs  $x$ , whereas the dashed line is the reverse ( $x$  to  $y$  and  $y$  to  $x$ ) of the least square fit of  $x$  vs  $y$ .

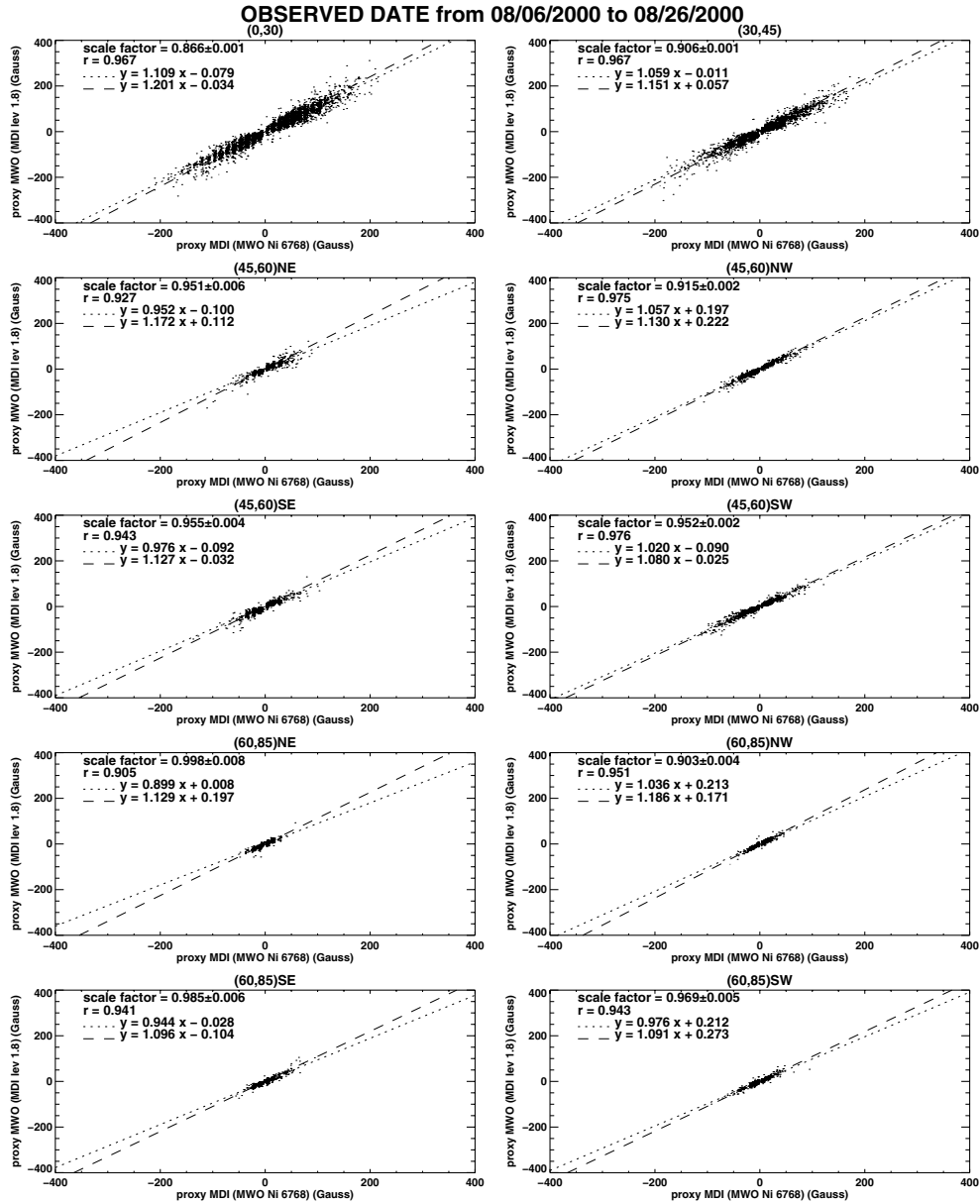


Fig. 12.— The scatter plots of groups of magnetograms from 6 Aug, 2000 to 26 Aug, 2000. The format here is the same as figure 11. Note that the correlations between different regions are now about the same.

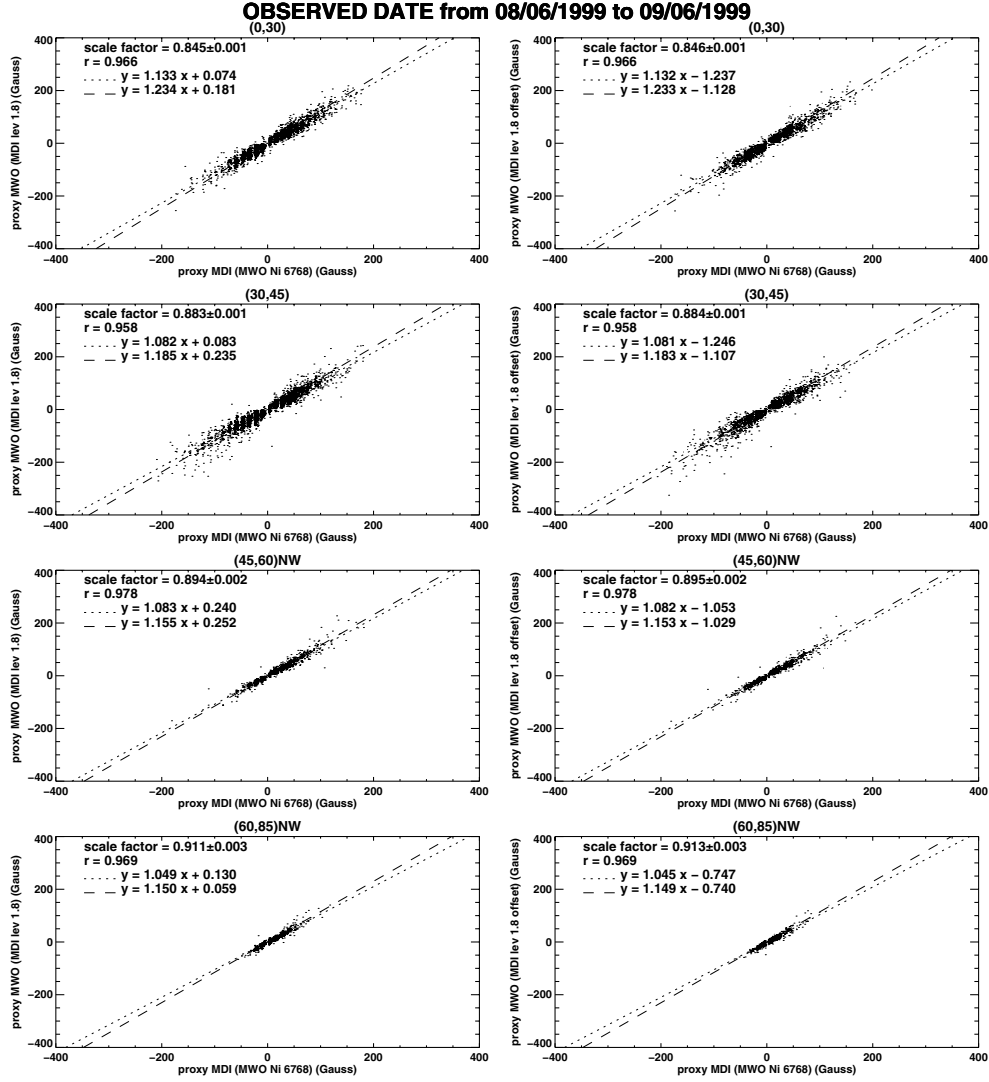


Fig. 13.— Sensitivity of the scale factor to the zero point shift detected in full-disk magnetograms obtained by MDI. The results shown on the left panels were obtained without any correction for this offset, while the right panels show the value of the scale factor calculated by correcting for this effect. The offset does not produce any significant effect on the calculated scale factor.